Fire Technology

DOI: 10.1007/s10694-014-0411-8

Experimental Study of Firebrand Transport

Kuibin Zhou, Jiangsu Key Laboratory of Hazardous Chemicals Safety and Control, College of Urban Construction and Safety Engineering, Nanjing Tech University, Nanjing 210009, Jiangsu, People's Republic of China; State Key Laboratory of Fire Science, University of Science and Technology of China, Hefei 230026, Anhui, People's Republic of China

Sayaka Suzuki, National Research Institute of Fire and Disaster (NRIFD), 4-35-3, Jindaiji Higashimachi, Chofu, Tokyo 182-0012, Japan

Samuel L. Manzello, Fire Research Division, National Institute of Standards and Technology (NIST), Gaithersburg, MD 20899, USA*

Received: 25 April 2014/**Accepted:** 27 April 2014

Abstract. The NIST Firebrand Generator (NIST Dragon) has been used to quantify the vulnerability of structures to ignition by firebrand attack. The Firebrand Generator is a useful device to study firebrand transport, and has been used to validate transport models of firebrand showers. During this series of experiments, the Firebrand Generator was fed with wood cubes of uniform size. The glowing firebrands generated were collected in an array of water-filled pans that were arranged to collect the bulk of the lofted firebrands. The pan arrangement was determined from repeated preliminary studies. These experiments were performed over a range of wind speeds (up to 9 m/s) to determine the lofting distance. The major change in these experiments from prior work was that, for a given wind speed, the firebrand size and mass was determined at each pan location. In the past, it was only possible to determine the number distribution; specifically the number of firebrands at each spatial location was counted (not resolved at every pan but only across a given row of pans). Statistical analysis indicated that a normal distribution was able to capture the number/mass percentage versus horizontal distance. This study provides even greater fidelity measurements to validate transport models of firebrand showers, and further insights into firebrand generation.

Keywords: Firebrands, WUI fires, Firebrand transport

1. Introduction

Firebrands are generated as vegetation and structures burn, and considered to be a major cause of structural ignition by analysis of post-fire damage assessments in Wildland Urban Interface (WUI) fires. During the Grass Valley fire, 199 homes were destroyed or damaged in which 193 ignited partly due to firebrand attack [1]. Direct and indirect firebrand attack was responsible for the ignition of 2/3 of destroyed homes in the Guejito and Witch fires [2].

* Correspondence should be addressed to: Samuel L. Manzello, E-mail: samuelm@nist.gov

Published online: 27 May 2014

A simplified methodology is to break the firebrand phenomenon into three main components: generation, transport, and ignition of exposed fuel. Most studies have focused on firebrand transport, including its trajectory of lofting from the fire plume, and how far it flies in the air (spotting distance) [3–9]. However, there is still limited literature on firebrand generation from vegetation and structures [10–15], as well as ignition of recipient fuel due to firebrand attack [16–19]. Furthermore, the transport mechanism of a single firebrand can be quantitatively described by physical models (dynamic model, combustion model, etc.), while the statistical approach is advised to analyze the data of firebrand generation and fuel ignition [20], mainly due to the complexity and uncertainty of firebrand showers in actual fires. In practice, a pragmatic approach to mitigate firebrand ignition of structures in WUI fires is to design homes that are more resistant to firebrand showers, thereby developing science-based building codes and standards for new construction in high risk areas. These needs stimulated the creation of a Firebrand Generator that could generate a controlled flux of glowing firebrand showers with a repeatable size and mass distribution [21, 22]. In conjunction with the Fire Research Wind Tunnel Facility (FRWTF) at the Building Research Institute (BRI) in Japan, the Firebrand Generator can direct this firebrand flux onto structural elements to evaluate their resistance to ignition [22].

The Firebrand Generator is also a useful device to study the transport of firebrand showers, and has been used to validate transport models [23]. The transport characteristics of firebrand showers are the focus of this paper. To this end, an experimental study was conducted on the mass and size of firebrands produced from this Firebrand Generator loaded with cube wood pieces, as compared to cylinders, and disks in previous work [21]. The major change in these experiments from prior work was that the firebrand size and mass was determined at each pan location. In previous work, it was only possible to determine the number distribution; specifically the number of firebrands at each spatial location was counted (not resolved at every pan but only across a given row of pans). The effect of the initial input condition on the mass distribution is presented, followed by a discussion of the influence of wind speed.

2. Experimental Description

Figure 1 is a drawing of the NIST Firebrand Generator. A brief description of the device is provided here since a detailed description has been provided elsewhere [21, 22]. This version of the device was scaled up from a first-generation, proof-of-concept Firebrand Generator [21]. The bottom panel displays the procedure for loading the wood cubes into the apparatus.

The wood cubes (11% moisture content on dry basis), 2.1 kg in total mass, were deposited into the Firebrand Generator by removing the top portion. The wood pieces were supported using a stainless steel mesh screen (0.35 cm spacing), which was carefully selected. The Firebrand Generator was driven by a 1.5 kW blower. After the wood cubes were loaded, the top section of the Firebrand Generator was coupled to the main body of the apparatus. The blower was then

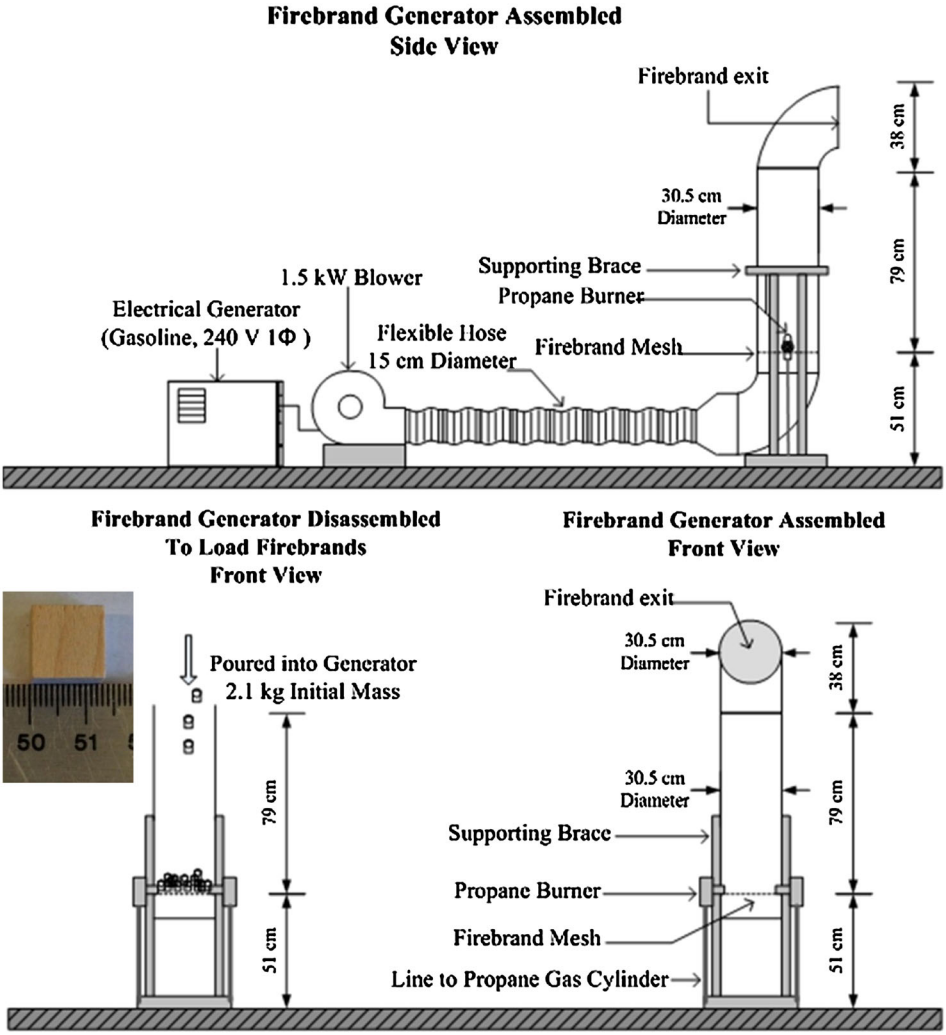

Figure 1. Schematic of the NIST Firebrand Generator (NIST Dragon).

switched to provide a low flow for ignition. The two propane burners were then ignited individually and simultaneously inserted into the side of the Firebrand Generator. This sequence of events was selected in order to generate a continuous flow of glowing firebrands for up to 4 min duration.

The Firebrand Generator was installed inside the FRWTF at BRI. A schematic of the facility is displayed in Figure 2a. The facility was equipped with a 4.0 m fan used to produce the wind field and was capable of producing up to a 10 m/s wind flow. The location of the Firebrand Generator is shown. To track the evolution of the size and mass distribution of firebrands produced, a series of water-filled pans was placed downstream of the Firebrand Generator (see Figure 2b). A

total of 277 rectangular pans were arranged in 40 rows and filled with water to quench burning firebrands. Each pan was 49.5 cm long and 29.5 cm wide. The arrangement and width of the pans was not random; rather it was based on scoping experiments to determine locations where the firebrands would most likely land. In comparison with [21], the Firebrand Generator was raised by 0.5 m off the ground, and the test section was extended by 9.85 m to accommodate more collection pans.

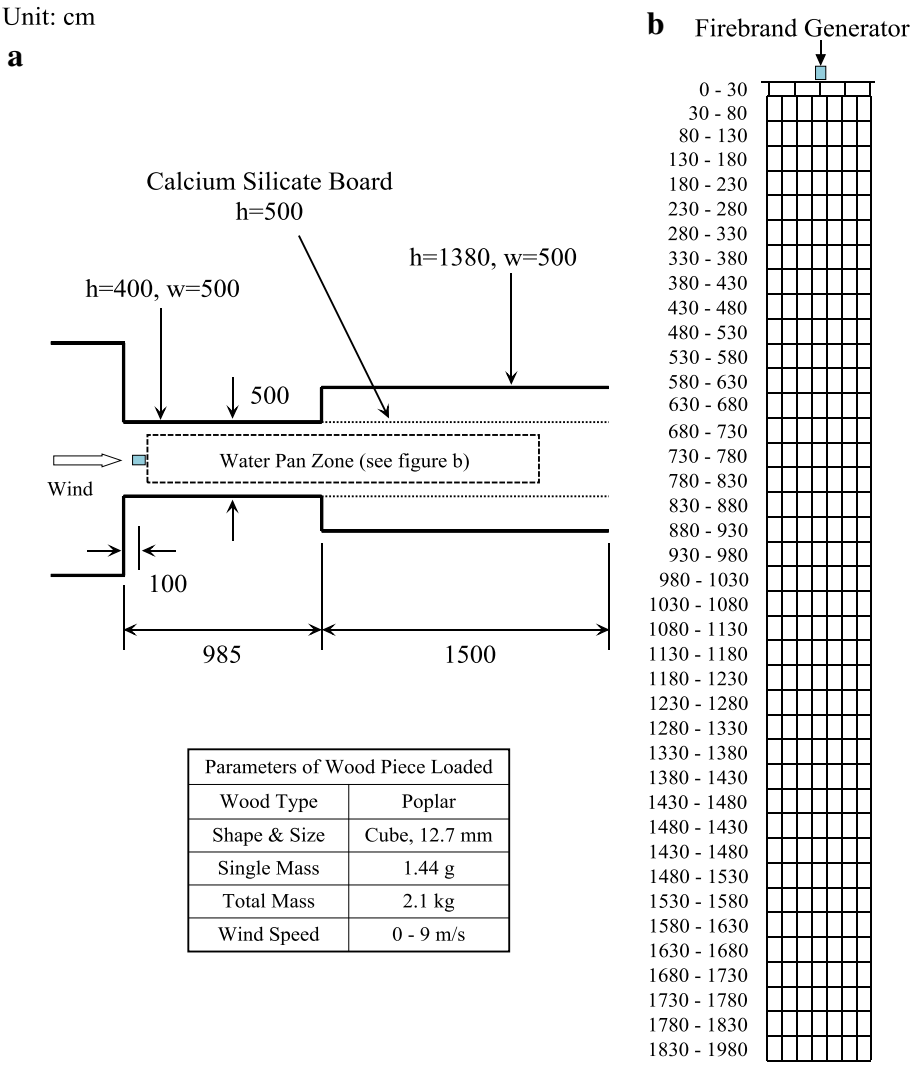

Parameters of Wood Piece Loaded	
Wood Type	Poplar
Shape & Size	Cube, 12.7 mm
Single Mass	1.44 g
Total Mass	2.1 kg
Wind Speed	0 - 9 m/s

Figure 2. (a) Schematic of the FRWTF. (b) Layout of pans used to collect the firebrands produced from the Firebrand Generator.

After each test, the firebrands were filtered from the water using a series of fine mesh, and then dried in an oven at 104°C for 8 h. The mass of each firebrand was measured by a precision balance with 0.001 g resolution. Repeat measurements of known calibration masses were measured by the balance which was used for the firebrand mass analysis. The standard uncertainty in the firebrand mass was approximately ±1%.

Image analysis software was used to determine the projected area of a firebrand by converting the pixel area using an appropriate scale factor [14]. It was assumed that deposited firebrands would rest flat on the ground and the projected areas with the maximum dimension and the second maximum dimension of three dimensions were measured (for cylindrical and flat shaped firebrands respectively) [14]. Images of well-defined shapes (e.g. circular objects) were used to determine the ability of the image analysis method to calculate the projected area [14]. Based on repeat measurements of different areas, the standard uncertainty in determining the projected area was ±10%.

A precision caliper with 1/1000 mm resolution was used to measure the thickness of each firebrand in the direction perpendicular to the projected area. For all the analyses in this study, the projected area and thickness were the maximum values for each firebrand. About 15,000 collected firebrands were sized and weighed.

3. Result and Discussion

3.1. Effect of the Loaded Wood Piece Under Baseline (No Wind Conditions; 0 m/s)

Manzello et al. [21] presented the mass distribution of firebrands produced from wood pieces of two different size cylinders, and one disk shape. In that work, the size of each individual wood piece, and initial mass, prior to combustion inside the Firebrand Generator were: first cylindrical wood piece was 8 mm in diameter, and 50 mm in length with mass being 1.29 g; second cylindrical wood piece was 12.5 mm in diameter, and 50 mm in length with mass being 3.14 g; and the disk wood piece was 25 mm in diameter, and 6 mm in length with mass being 1.56 g. In turn, the total mass of firebrands collected, under no wind speed (0 m/s wind tunnel speed; simply propelled by the fan of the Firebrand Generator), was 57 g, 43 g and 44 g, respectively corresponding to 8.1, 6.1 and 6.3% of the initial mass converted into firebrands (700 g was the total initial wood mass of each of the three geometries loaded in all cases). In comparison, in this study, the initial size and mass of a cube wood piece was 12.7 mm in width, with mass being 1.44 g, and the ratio of the total firebrand mass generated to the total loaded wood pieces mass was 4.4% (2.1 kg was the total initial wood mass of the cube pieces, as indicated that the Firebrand Generator used in this study was larger than prior work [21]). This suggests that the mass, shape, and wood type of the initially loaded wood pieces influenced the conversion of virgin wood to firebrands inside the Firebrand Generator.

Figure 3 shows the mass distribution of firebrands produced from the Firebrand Generator fed with four different wood pieces described above under 0 m/s wind speed. In order to provide a better understanding of the influence of initial shape on firebrand production, the dimensionless mass, normalized by the single initial wood piece mass of each geometry, used was applied to the histogram distribution. As shown in Figure 4, 86% of the firebrands produced when cubes are used were less than 2% of the initial mass of a single wood piece, whereas when disks are used, 45% of firebrands were over 5% of the mass. Thus, the shape of the loaded wood piece was an important parameter affecting the firebrand mass distribution. It is essential to mention that the wood (poplar) density was approximately 700 kg/m^3 in this study, which is larger than that of ponderosa pine wood in the previous work [21]. In general, the charring rate of wood decreases as its density increases [24], which indicates that the poplar wood piece should lose much more mass than the ponderosa wood pieces if both pieces are same in size and shape. Thus, the cube shape showed more mass loss due to combustion.

3.2. The Wind Speed Effect (Only Cube Wood Piece Considered)

The total mass of firebrands generated was measured as a function of wind speed. When the wind speed was increased from 0 m/s to 9 m/s, the total firebrand mass was measured as 93 g, 57 g and 63 g, respectively, and corresponded to 4.4% (at 0 m/s), 2.7% (at 6 m/s) and 3.0% (at 9 m/s) of the total wood pieces loaded.

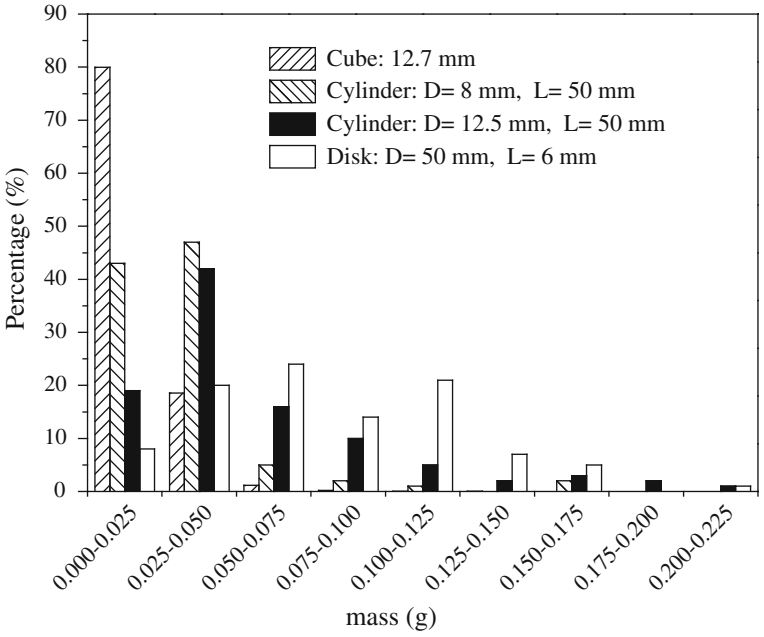

Figure 3. Mass distribution of firebrands generated from wood pieces of different shapes under no wind.

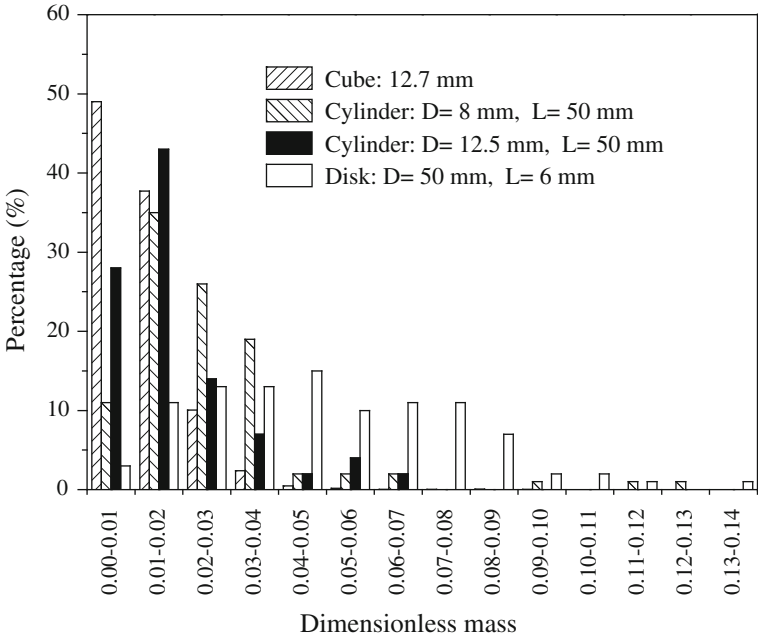

Figure 4. Dimensionless mass distribution of firebrands generated for different shapes under no wind.

From video records, some firebrands were lofted outside the measurement location (downstream) at 6 m/s and 9 m/. In addition, it is possible that several firebrands were also burned completely before reaching the pans at the higher velocities. The reduction in mass at 6 m/s and 9 m/s must have been due to a combination of these effects. It is interesting to observe that no significant change was observed in the total mass of firebrands collected as the wind speed was increased from 6 m/s to 9 m/s. Yet, as shown in Figure 5, the percentage of firebrands within the range of 0% to 1% of the initial mass was the largest under 9 m/s wind speed, whereas the 0 m/s situation held the largest percentage of mass firebrands within the range of 1% to 2%, and the percentages were nearly the same in other ranges.

The average mass of each firebrand produced was 17 mg ± 12 mg (0 m/s; average ± standard deviation), 15 mg ± 14 mg (6 m/s), and 15 mg ± 11 mg (9 m/s). The average projected area of each firebrand produced was 0.37 ± 0.17 cm^2 (0 m/s), 0.33 ± 0.18 cm^2 (6 m/s), and 0.34 ± 0.16 cm^2 (9 m/s). The thickness of each firebrand produced was 0.35 ± 0.29 cm (0 m/s), 0.33 ± 0.16 cm (6 m/s), and 0.33 ± 0.12 cm (9 m/s). It is interesting to observe that little or no change was also observed in the average mass, and projected area of each firebrand generated as the wind speed increased from 6 m/s to 9 m/s.

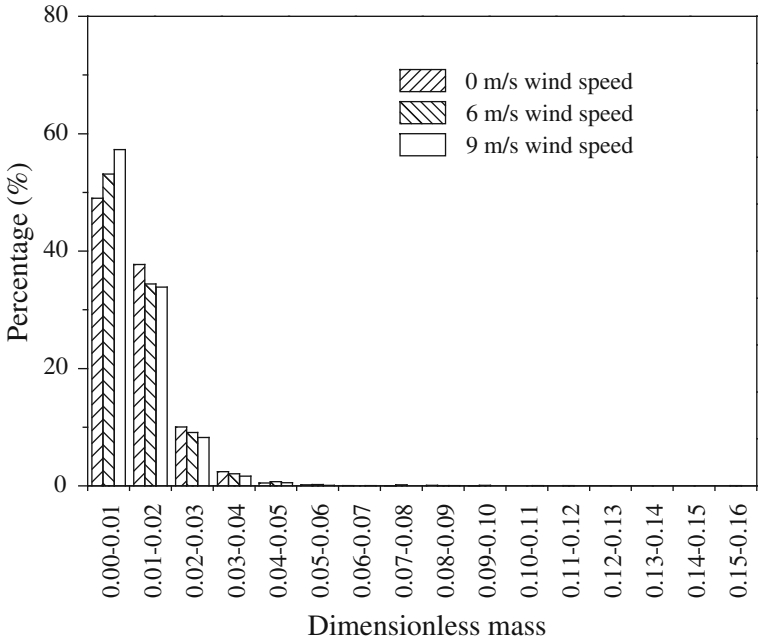

Figure 5. Comparison of the dimensionless mass distribution under different wind speed. The dimensionless mass is scaled by the initial wood piece mass, i.e. 1.44 g.

3.2.1. Effect of Wind Speed on the Number/Mass Percentage Versus Distance. As the wind increased, the firebrand hazard enhances in all respects, intensifying firebrand generation, transport, and ignition of recipient fuels [22]. Firebrands can be transported further by stronger wind, for the absolute velocity of firebrand could reach the wind speed in the horizontal direction after a short while [3]. In this study, the wind speed determined the maximum distance that the firebrand traveled, as well as the landing range of the maximum number/mass percentage. As shown in Figs. 6 and 7, the firebrands were collected as far as 3.3 m, 7.3 m, and 11.8 m under the effect of 0 m/s, 6 m/s and 9 m/s wind speed, respectively. The landing regimes of maximum number percentage are 0.8 m to 1.3 m, 1.3 m to 1.8 m, and 2.8 m to 3.3 m for 0 m/s, 6 m/s and 9 m/s wind speed, respectively. It is of great interest to note that the profile of the number/mass percentage versus distance scattered smoothly as the wind speed increases.

In order to mathematically quantify the wind effect, the Gaussian function (i.e. normal distribution) was tested for depicting the number/mass percentage versus distance as follows:

$$\lim_{x\to 0}\frac{y}{x} \equiv f(x) = \frac{1}{\sqrt{2\pi}w}\exp\left(-\frac{(x-x_c)^2}{2w^2}\right) \tag{1}$$

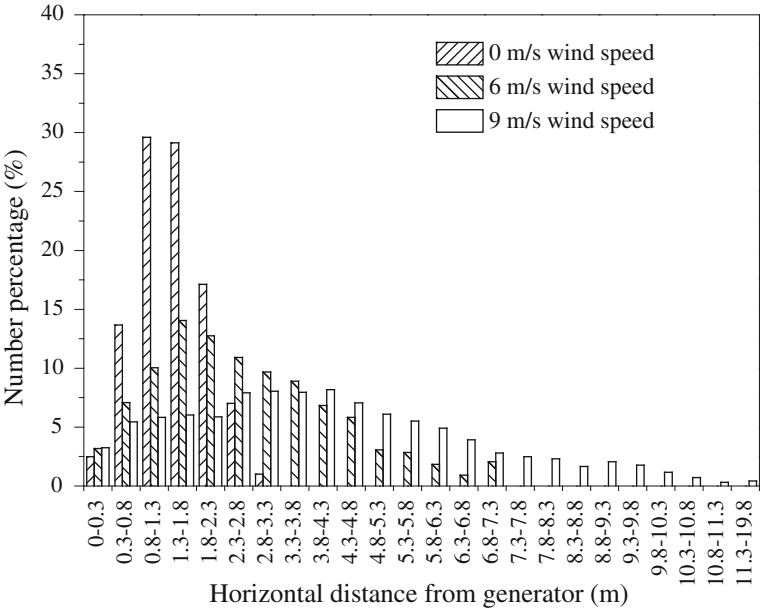

Figure 6. Comparison of the number percentage versus distance under different wind speeds.

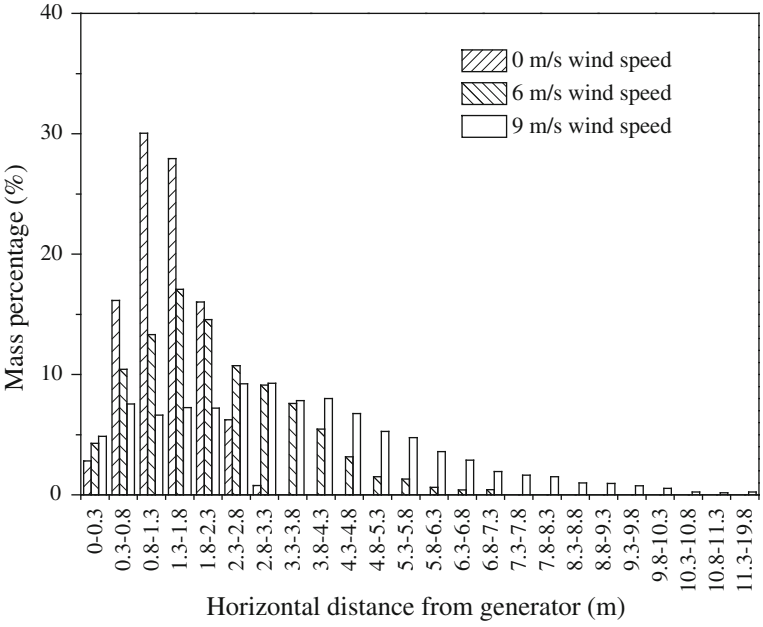

Figure 7. Comparison of the mass percentage versus distance under different wind speeds.

where y is the number/mass percentage; x is the horizontal distance away from the Firebrand Generator; x_c and w are two parameters, respectively denoting the center and width of the distribution profile. If the random variable X is used to present the horizontal distance of the firebrand away from the Firebrand Generator, x_c, w and $f(x)$ should be the expected value, root-mean-square deviation, and probability density function of X. Thus x_c and w can be approximately determined by the formula:

$$x_c \approx E(X) = \sum_{i=1}^{m} x_i y_i \tag{2}$$

$$w \approx \sqrt{D(X)} = \sqrt{\sum_{i=1}^{m} x_i^2 y_i - (E(X))^2} \tag{3}$$

where x_i is the distance of the center of collected pans in the ith row away from the Firebrand Generator, and y_i is the corresponding number/mass percentage of firebrands collected by the ith row pan, and m is the number of rows. For the number percentage distribution, x_c is calculated to be 1.40 (0 m/s), 2.69 (6 m/s), and 4.21 (9 m/s), with the w being 0.61, 1.61 and 2.52, respectively. For the distribution of mass percentage, x_c and w are 1.35 and 0.61 (0 m/s), 2.20 and 1.36 (6 m/s), 3.49 and 2.30 (9 m/s). As shown in Figs. 8 and 9, a Gaussian function can capture y/A versus x without wind, where A is the pan width of each row. The situation with wind also can be described by Equation (1). Note that A equals 0.3 m for the first row and 0.5 m for others, and that the theoretical curve could fit though (0, 0) as A is small enough for the calculated x_c and w to approach the true value.

This approximate normal distribution may be physically explained by the central limit theorem in probability theory [25]. In more detail, $X = \frac{1}{n}\sum_{j=1}^{n} X_j$ where n is the number of firebrands collected which is large enough for each test to satisfy the central limit theorem and X_j is the random variable presenting the jth firebrand, and X_j (j = 1, 2…) are assumed to be independent on each other but with the same expectation and variance. Thus, the effect of wind speed on the number/mass percentage versus distance can be quantified by the expectation x_c and root-mean-square deviation w, both of which are nonlinearly proportional to the wind speed as evidenced by the above calculation.

3.2.2. Effect of Wind Speed on the Mass Versus Projected Area. Figure 10 presents the distribution of mass versus projected area of firebrands obtained in this study under different wind speeds. The slope of mass versus projected area is 0.48, 0.51, and 0.48 with zero intercept for the situations of 0 m/s, 6 m/s and 9 m/s wind speed, respectively. However, the variation of mass, at a certain projected area, appeared to lessen to a small extent as the wind speed increased. It seems that the

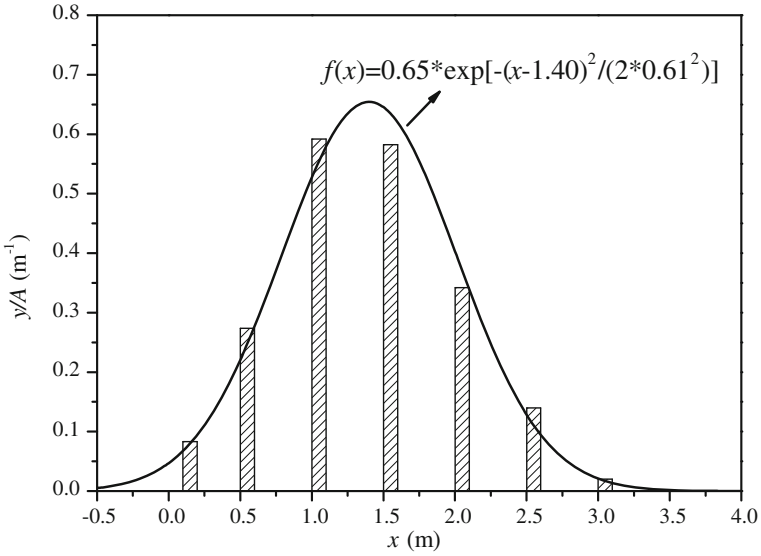

Figure 8. Comparison in number percentage between experimental data and Gaussian function under no wind.

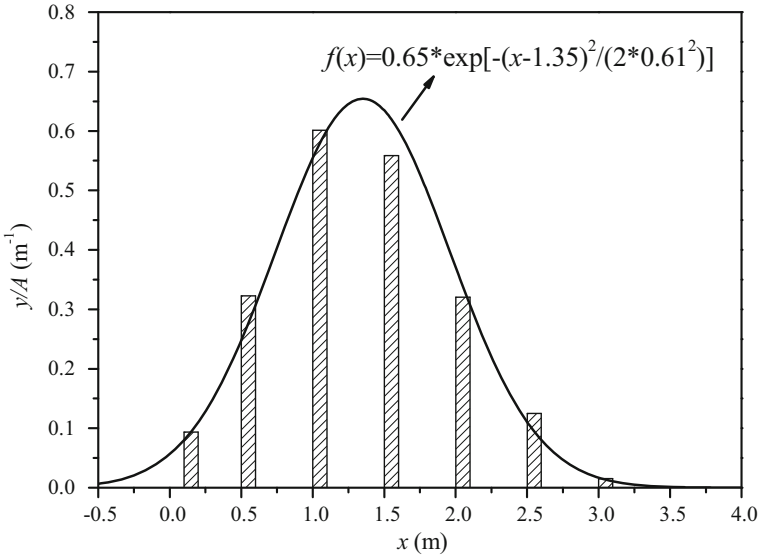

Figure 9. Comparison in mass percentage between experimental data and Gaussian function under no wind.

wind speed had little effect on the distribution of mass versus projected area, although the mass distribution was considerably affected by the wind speed. It can be deduced that the wind speed also holds an important role in the distribution of projected area.

3.2.3. Effect of Wind Speed on the Thickness Versus Square Root of Projected Area. The firebrand size can be quantitatively determined by diameter for sphere firebrands, and diameter and length, for cylinder, and disk shaped firebrands. Together with the projected area, the thickness helps depict the three dimensional nature of flat-shaped firebrands. As shown in Figure 11, the slope of the thickness versus square root of projected area was 0.58, 0.59 and 0.57, with zero intercept for the situations of 0 m/s, 6 m/s and 9 m/s wind speed, respectively. The variation of thickness at the square root of a certain projected area decreased to a considerable extent as the wind speed increased. Firebrands, whose square root of projected area is more than the thickness, accounts for 98, 99, and 99% of all firebrands under the effect of 0 m/s, 6 m/s and 9 m/s wind speed, respectively. Therefore, the wind speed had little effect on the distribution of the thickness versus square root of projected area, similar to that of the mass versus projected area. It also can be found that most of firebrands produced when the Firebrand Generator was fed with cube wood piece cannot be assumed to be of cube shape, different from the situations of cylindrical and disk wood piece [21].

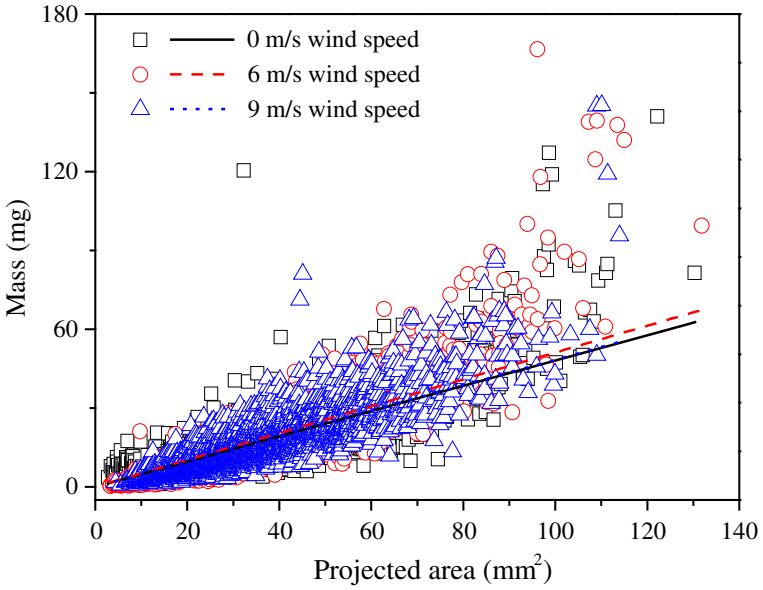

Figure 10. Distribution of the mass versus projected area under different wind speeds.

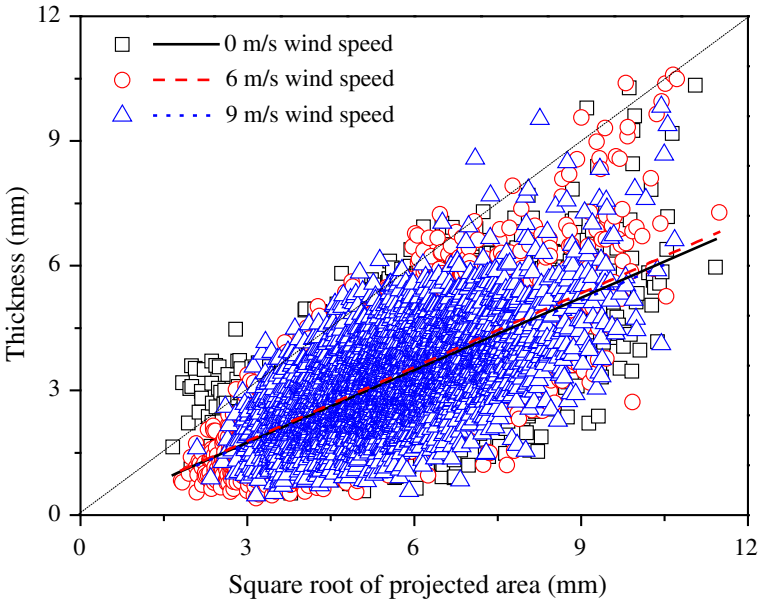

Figure 11. Distribution of the upright thickness versus square root of projected area under different wind speeds.

4. Summary

This paper presents a systematic study on the character of firebrands produced from the Firebrand Generator loaded with cube wood pieces under the effect of different wind speeds. The main conclusions are listed as follows:

(1) The mass and shape of the initial wood piece fed into the Firebrand Generator, as well as the wind speed, had a significant effect on the mass distribution of firebrands generated.
(2) The profile of the number/mass percentage versus horizontal distance was considerably affected by the wind speed, and was quantitatively described by a Gaussian function (i.e. normal distribution), with both expectation, and root-mean-square deviation nonlinearly proportional to the wind speed.
(3) The wind speed had little effect on the distribution of both the mass versus projected area and the thickness versus the square root of the projected area.

Acknowledgements

KZ acknowledges support by the National Natural Science Foundation of China under Grant 51120165001 and Open Project of State Key Laboratory of Fire Science HZ2013-KF09. SLM is thankful to BRI for allowing NIST to use the FRWTF for these experiments.

References

1. Cohen JD, Stratton RD (2008) Home destruction examination: Grass Valley Fire, Lake Arrowhead, California. Pacific Southwest Region (Region 5), Forest Service, U.S. Department of Agriculture, Vallejo, CA
2. Maranghides A, Mell W (2011) A case study of a community affected by the witch and Guejito wildland fires. Fire Technol 47(2):379–420. doi:10.1007/s10694-010-0164-y
3. Tarifa CS, Notario PPd, Moreno FG (1965) On the flight paths and lifetimes of burning particles of wood. Proc Combust Inst 10(1):1021–1037. doi:10.1016/s0082-0784(65)80244-2
4. Lee S-L, Hellman JM (1969) Study of firebrand trajectories in a turbulent swirling natural convection plume. Combust Flame 13(6):645–655. doi:10.1016/0010-2180(69)90072-8
5. Lee SL, Hellman JM (1970) Firebrand trajectory study using an empirical velocity-dependent burning law. Combust Flame 15(3):265–274. doi:10.1016/0010-2180(70)90006-4
6. Muraszew A, Fedele JB, Kuby WC (1977) Trajectory of firebrands in and out of fire whirls. Combust Flame 30:321–324. doi:10.1016/0010-2180(77)90081-5
7. Albini FA (1979) Spot fire distance from burning trees: a predictive model. Intermountain Forest and Range Experiment Station, Forest Service, U.S. Department of Agriculture
8. Albini FA (1981) Spot fire distance from isolated sources: extensions of a predictive model. Intermountain Forest and Range Experiment Station, Forest Service, U.S. Department of Agriculture
9. Albini FA (1983) Transport of firebrands by line thermals. Combust Sci Technol 32(5–6):277–288. doi:10.1080/00102208308923662
10. Waterman T (1969) Experimental study of firebrand genenration. Engineering Mechanics Division, IIT Research Institution
11. Yoshioka H, Hayashi Y, Masuda H, Noguchi T (2004) Real-scale fire wind tunnel experiment on generation of firebrands from a house on fire. Fire Sci Technol 23(2):142–150
12. Manzello SL, Maranghides A, Mell WE (2007) Firebrand generation from burning vegetation. Int. J. Wildland Fire 16(4):458–462. doi:10.1071/WF06079
13. Manzello SL, Maranghides A, Shields JR, Mell WE, Hayashi Y, Nii D (2009) Mass and size distribution of firebrands generated from burning Korean pine (Pinus koraiensis) trees. Fire Mater 33(1):21–31. doi:10.1002/fam.977
14. Suzuki S, Manzello SL, Lage M, Laing G (2012) Firebrand generation data obtained from a full-scale structure burn. Int. J. Wildland Fire 21(8):961–968. doi:10.1071/WF11133
15. Suzuki S, Manzello SL, Hayashi Y (2013) The size and mass distribution of firebrands collected from ignited building components exposed to wind. Proc. Combust 34(2):2479–2485. doi:10.1016/j.proci.2012.06.061
16. Dowling VP (1994) Ignition of timber bridges in bushfires. Fire Saf J 22(2):145–168. doi:10.1016/0379-7112(94)90070-1
17. Manzello SL, Cleary TG, Shields JR, Yang JC (2006) On the ignition of fuel beds by firebrands. Fire Mater 30(1):77–87. doi:10.1002/fam.901
18. Manzello SL, Cleary TG, Shields JR, Yang JC (2006) Ignition of mulch and grasses by firebrands in wildland-urban interface fires. Int. J. Wildland Fire 15(3):427–431. doi:10.1071/wf06031
19. Viegas DX, Almeida M, Raposo J, Oliveira R, Viegas CX (2012) Ignition of mediterranean fuel beds by several types of firebrands. Fire Technol 50(1):1–17. doi:10.1007/s10694-012-0267-8

20. Koo E, Pagni PJ, Weise DR, Woycheese JP (2010) Firebrands and spotting ignition in large-scale fires. Int. J. Wildland Fire 19(7):818–843. doi:10.1071/WF07119
21. Manzello SL, Shields JR, Cleary TG, Maranghides A, Mell WE, Yang JC, Hayashi Y, Nii D, Kurita T (2008) On the development and characterization of a firebrand generator. Fire Safety J. 43(4):258–268. doi:10.1016/j.firesaf.2007.10.001
22. Manzello SL, Suzuki S, Hayashi Y (2012) Enabling the study of structure vulnerabilities to ignition from wind driven firebrand showers: a summary of experimental results. Fire Safety J. 54:181–196. doi:10.1016/j.firesaf.2012.06.012
23. Kortas S, Mindykowski P, Consalvi JL, Mhiri H, Porterie B (2009) Experimental validation of a numerical model for the transport of firebrands. Fire Safety J. 44(8):1095–1102. doi:10.1016/j.firesaf.2009.08.001
24. Cachim P, Franssen J-M (2010) Assessment of Eurocode 5 charring rate calculation methods. Fire Technol 46(1):169–181. doi:10.1007/s10694-009-0092-x
25. Loeve M (1950) Fundamental limit theorems of probability theory. Ann Math Stat 21(3):321–338. doi:10.2307/2236489